Biogeosciences Discuss., doi:10.5194/bg-2016-118, 2016
Manuscript under review for journal Biogeosciences
Published: 11 July 2016

Biogeosciences Discussions Open Access EGU

Depth-averaged instantaneous currents in a tidally dominated shelf sea from glider observations

Lucas Merckelbach[1]

[1]Helmholtz Zentrum Geesthacht, Centre for Coastal Research, Geesthacht, Germany.

Correspondence to: Lucas Merckelbach (lucas.merckelbach@hzg.de)

Abstract. Ocean gliders have become ubiquitous observation platforms in the ocean in recent years. They are also increasingly used in coastal environments. The coastal observatory system COSYNA has pioneered the use of gliders in the North Sea, a shallow tidally energetic shelf sea.

For operational reasons, the gliders operated in the North Sea are programmed to resurface every 3-5 hours. The glider's deadreckoning algorithm yields depth averaged currents, averaged in time over each subsurface interval. Under operational conditions these averaged currents are a poor approximation of the instantaneous tidal current.

In this work an algorithm is developed that estimates the instantaneous current (tidal and residual) from glider observations only. The algorithm uses a second-order Butterworth low-pass filter to estimate the residual current component, and a Kalman filter based on the linear shallow water equations for the tidal component. A comparison of data from a glider experiment with current data from an ADCP deployed nearby shows that the standard deviations for the east and north current components are better than 7 $\mathrm{cm \cdot s^{-1}}$ in near-real time mode, and improve to better than 5 $\mathrm{cm \cdot s^{-1}}$ in delayed mode, where the filters can be run forward and backward.

In the near-real time mode the algorithm provides estimates of the currents that the glider is expected to encounter during its next few dives. Combined with a behavioural and dynamic model of the glider, this yields predicted trajectories, the information of which is incorporated in warning messages issued to ships by the (German) authorities. In delayed mode the algorithm produces useful estimates of the depth averaged currents, which can be used in (process-based) analyses in case no other source of measured current information is available.

1 Introduction

Ocean gliders, or gliders for short, have become ubiquitous observation platforms in the ocean in recent years. In the Coastal Observing SYstem for Northern and Arctic seas observatory system, COSYNA, (Baschek et al., 2016) the use of Teledyne Webb Research Slocum electric gliders has been pioneered in the North Sea, a tidally energetic shelf sea. The gliders operated within COSYNA are equipped with CTD, optical backscatter, fluorescence and microstructure sensors, intended to observe more or less directly parameters such as temperature, salinity, (proxies for) suspended sediment (via optical backscatter) and chlorophyll a concentrations (via fluorescence), and turbulence dissipation rates.

Biogeosciences Discuss., doi:10.5194/bg-2016-118, 2016
Manuscript under review for journal Biogeosciences
Published: 11 July 2016

Gliders have found application in a wide range of research topics, see (Rudnick, 2016) for a recent review. In particular the availability of small size and low power optical backscatter and fluorescence sensors makes gliders suitable for studies on biochemical processes. For example, the occurrence of phytoplankton blooms is strongly influenced by mixing, as mixing affects light conditions and nutrient budgets in the water column.(e.g., Xu et al., 2013). The structure of the water column in shelf seas such as the North Sea, is a balance between stabilising surface heating, and destabilising turbulence generated by shear close to the sea bed and at the surface by tidal currents and wind driven currents, respectively (Simpson and Hunter, 1974). In addition, pelagic mixing caused by shear across the thermocline couples the euphotic and the eutrophic zones above and below the thermocline, and therefore has an important effect on the benthic and pelagic foodweb (Rippeth et al., 2005). Consequently, the analysis and interpretation of the biochemical parameters measured by the glider, requires understanding of the mixing, which in shelf seas, in turn depends strongly on tidal and wind driven currents.

Shelf seas are often shallow enough that tidal and wind driven currents lead to resuspension and deposition events of sediment (Glenn et al., 2008; Tropp, 2013). Similar to fluorescence sensors, optical backscatter or turbidity sensors are commonly fitted to gliders, often even in the same housing. Optical backscatter intensity, when calibrated against filtrated water samples, is a proxy for sediment concentration. Also here, the analysis and interpretation of resuspension events and transport of suspended sediments requires information on the local currents.

Although currents can be measured from gliders using low power acoustic Doppler current profilers (ADCPs) (Johnston et al., 2013), their high cost and (still) relatively high power consumption makes the use of ADCPs on gliders prohibitive, except for dedicated experiments. Instead, moored or shipborn ADCPs could be used, however, this would restrict the moving space of the glider, or the currents measured would not co-locate with the glider data. Alternatively current estimates from the glider itself, resulting from its navigation algorithm could be used (Section 2). However, the loss of information due to averaging in time can become substantial in situations when subsurface times become of the same order of magnitude as the time scale of the variability of the current. As an example, in the North Sea, which is dominated by the semidiurnal M2 tide, the current reverses every 6 hours or so. During glider operations the typical subsurface time is about 3 hours, and therefore poorly resolves the tidal variability.

From an operational point of view, any significant variation in the currents that, from a glider's perspective, appears to have a time scale that is similar to its subsurface time, will cause it to have trouble maintaining the pre-programmed course. Methods have been developed in order to plan trajectories for optimal sampling purposes (e.g., Garau et al., 2009), or to reconstruct the underwater trajectory to localise the data that are gathered by the glider (e.g., Smith et al., 2010). The source of information on the water motion is usually an ocean current model. Elaborating on this work, Smith et al. (2012) developed a system aiming at the effective execution of a planned path, that is, designing the mission such that the glider is capable of travelling along the planned path within given constraints. Effective execution also improves safety at sea, as smaller regions can be defined where gliders can be present.

Safety at sea is in fact a major aspect in glider operations with the COSYNA coastal observatory. Since glider operations take place mostly in the German sector of the North Sea, the planning and execution of glider missions need to comply with the regulations set by the governing German shipping authority Wasser- und Schifffahrtsamt (WSA). This involves the application

Biogeosciences Discuss., doi:10.5194/bg-2016-118, 2016
Manuscript under review for journal Biogeosciences
Published: 11 July 2016

for permission to run gliders in a given region within a certain time frame. Since there is a risk of a ship-glider collision (Merckelbach, 2013), which may damage vulnerable fast off-shore vessels (Drücker et al., 2015), WSA requires mitigating measures to be taken by providing the German Vessel Traffic Control Centre (Seewarndienst) with 12-hourly forecasts of the region where the glider will be, given by the four coordinates defining a rectangle. The system that has been set up to provide these forecasts (not discussed herein) relies on a model simulating the behaviour of the glider by emulating the glider software and hardware, as well as modelling the dynamics (*i.e.,* its flight through water). However, a realistic prediction requires information on the local currents up to 12 hours ahead.

In the present work ocean current models are not relied upon to provide information on the water motion. Instead, the aim is to reconstruct the instantaneous currents by recovering (most of) the information in the observed currents lost due to the time averaging.

To that end, an algorithm is proposed that is composed of a simple low pass filter for low frequency variations in the currents due to atmospheric influence, for example, and a Kalman filter based on the shallow water equations to estimate the tidally induced variation in the currents.

2 Depth and time averaged currents from the glider platform

The Teledyne Webb Research Slocum electric glider uses a dead-reckoning algorithm for underwater positioning. The algorithm combines the depth rate of change from the pressure transducer and heading and pitch from the attitude sensor to compute the horizontal velocity components. The dead-reckoned underwater position follows from integrating the current vectors with respect to time, starting from the latest known GPS position. The difference between the dead-reckoned resurface position and the actual GPS position is attributed to a depth and time averaged current, see also Merckelbach et al. (2008), for example. The glider user can define whether or not the glider navigation algorithm should apply this current estimate to compensate for drift when calculating the heading for the current waypoint during the next dive. Doing so only makes sense, however, when the time variability is sufficiently resolved.

3 An algorithm for short-time current estimates

Even though the currents in a coastal sea, as considered herein, are dominated by the tide, non-tidal currents due to atmospheric conditions and fresh water influx, for example, can have significant effects. In contrast to the tidal current components, the non-tidal components are hard to model without resorting to complex numerical models. The non-tidal currents *can* (but do not have to) vary on short time scales of the order of hours. Henceforth, for practical reasons, the currents are decomposed into a tidal component, consisting of at most a few of the main tidal constituents, and a slowly varying non-tidal component, or residual current.

Biogeosciences Discuss., doi:10.5194/bg-2016-118, 2016
Manuscript under review for journal Biogeosciences
Published: 11 July 2016

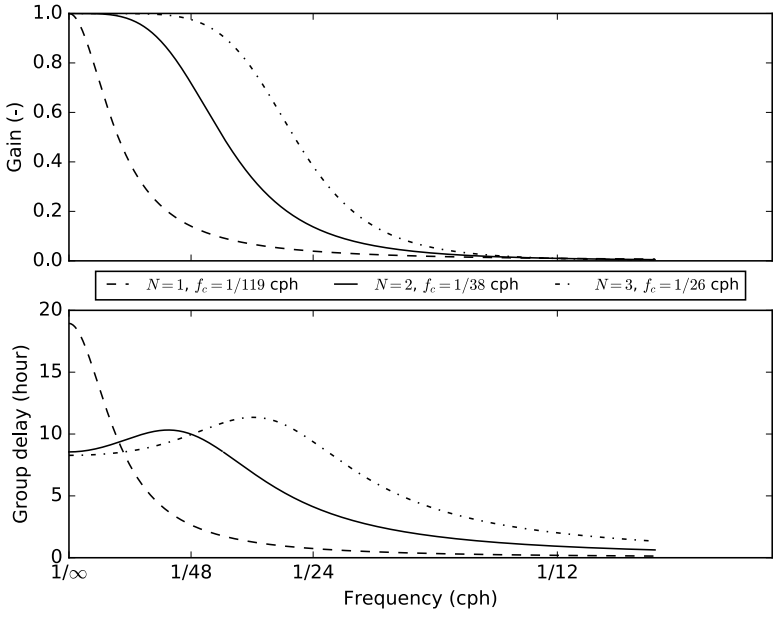

Figure 1. Filter responses of Butterworth filters of the first, second and third order. Top panel shows the gain as a function of frequency, and the bottom panel shows the group delay as a function of frequency.

3.1 Residual currents

Due to the stochastic character of the residual current components, a low pass filter is applied. In practice, the transition from pass to no-pass at the cut-off frequency (the transition band) is gradual. Furthermore, a low pass filter generally does not preserve the phase of the filtered signal and introduces a frequency dependent lag to the filtered signal (the group delay). For this purpose, an efficient low pass Butterworth filter is implemented (e.g., Oppenheim et al., 1997). The properties of the filter are determined by cut-off frequency f_c and its order. The order of the filter is a trade-off between the width of the transition band and the group delay. Figure 1 shows the filter responses of Butterworth filters of the order $N = \{1,2,3\}$. The top panel shows the (power) gain as a function of frequency. In order to effectively remove the main tidal signals (semidiurnal components and their higher harmonics), the cut-off frequency of each filter is chosen such that the gain of frequencies with a period of 12 hours or smaller have a gain less than 0.01, yielding cut-off frequencies of $f_c = \{1/119, 1/38, 1/26\}$ cph for $N = \{1,2,3\}$. It is clearly seen that with increasing order the transition band from pass to no-pass becomes smaller. A narrow transition band comes at a price of a large group delay (see bottom panel). The result is that features with a frequency in the pass-band are retained better, but appear with a significant delay. In practise this would mean that the algorithm would account for a transient feature, but with a given time delay yielding poor results through out the time span of the delay. As a compromise the filter is designed according to a second-order Butterworth filter.

Biogeosciences Discuss., doi:10.5194/bg-2016-118, 2016
Manuscript under review for journal Biogeosciences
Published: 11 July 2016

Since a low pass filter inevitably introduces a phase lag to the filtered signal, during post-processing the low pass filter can run first forwards and then backwards in time in order to compensate for phase lags. To mitigate as best as possible the transient effects at both boundaries, that are also inevitable, the time series is odd-padded by an equivalent of 12 hours of data points.

3.2 Tidal currents

In contrast to the residual currents, the evolution of tidal currents can be captured to a large extent by a simple model. In this section we will cast such a simple model into a Kalman filter to provide an optimal estimate of the tidal current components that the glider will face during its next dive, based on all previous depth and time-averaged water current data it has collected.

3.2.1 Intermezzo on Kalman filtering

For an introduction on Kalman filters and their derivation, the reader is referred to e.g. Simon (2006). Here, for the sake of brevity, we will state the general computational procedure only.

The Kalman filter is formulated as a dynamical system (Simon, 2006)

$$\begin{aligned}
\boldsymbol{x}_k &= \boldsymbol{F}_{k-1}\boldsymbol{x}_{k-1} + \boldsymbol{w}_{k-1} \\
\boldsymbol{y}_k &= \boldsymbol{H}_k\boldsymbol{x}_k + \boldsymbol{v}_k \\
\boldsymbol{w}_k &\approx \mathcal{N}\{0, \boldsymbol{Q}_k\} \\
\boldsymbol{v}_k &\approx \mathcal{N}\{0, \boldsymbol{R}_k\}
\end{aligned} \tag{1}$$

where $\boldsymbol{x}$ is the state vector, $\boldsymbol{F}$ the transition matrix, $\boldsymbol{y}$ the measurement vector, $\boldsymbol{H}$ the measurement matrix, $\boldsymbol{w}$ the process noise vector (normal distributed with zero mean and known variance $\boldsymbol{Q}_k$), $\boldsymbol{v}$ the measurement noise vector (normal distributed with zero mean and known variance $\boldsymbol{R}_k$) and k the measurement index number. If, for example, the state vector is composed of the eastward and northward velocity components, then the transition matrix describes how the currents would change from one time step k to the next. The measurement matrix relates the observed parameters, $\boldsymbol{y}$, to the state vector.

The procedure for the Kalman filter is given by the following equations for $k = 1, 2, 3, ...$

$$\boldsymbol{P}_k^- = \boldsymbol{F}_{k-1}\boldsymbol{P}_{k-1}^+\boldsymbol{F}_{k-1}^T + \boldsymbol{Q}_{k-1} \tag{2}$$

$$\boldsymbol{K}_k = \boldsymbol{P}_k^-\boldsymbol{H}_k^T(\boldsymbol{H}_k\boldsymbol{P}_k^-\boldsymbol{H}_k^T + \boldsymbol{R}_k)^{-1} \tag{3}$$

$$\hat{\boldsymbol{x}}_k^- = \boldsymbol{F}_{k-1}\hat{\boldsymbol{x}}_{k-1}^+ \tag{4}$$

$$\hat{\boldsymbol{x}}_k^+ = \hat{\boldsymbol{x}}_k^- + \boldsymbol{K}_k(\boldsymbol{y}_k - \boldsymbol{H}_k\hat{\boldsymbol{x}}_k^-) \tag{5}$$

$$\boldsymbol{P}_k^+ = (\boldsymbol{I} - \boldsymbol{K}_k\boldsymbol{H}_k)\boldsymbol{P}_k^-(\boldsymbol{I} - \boldsymbol{K}_k\boldsymbol{H}_k)^T + \boldsymbol{K}_k\boldsymbol{R}_k\boldsymbol{K}_k^T, \tag{6}$$

where $\hat{\boldsymbol{x}}_k^-$ is the *a priori* estimate, $\boldsymbol{P}_k^-$ the *a priori* covariance, $\hat{\boldsymbol{x}}_k^+$ the *a posteriori* estimate, and $\boldsymbol{P}_k^+$ the *a posteriori* covariance.

Biogeosciences Discuss., doi:10.5194/bg-2016-118, 2016
Manuscript under review for journal Biogeosciences
Published: 11 July 2016

The filter is initialised with estimates for

$$\hat{\boldsymbol{x}}_0^- = \hat{\boldsymbol{x}}_0, \text{ and} \tag{7}$$

$$\boldsymbol{P}_0^- = \boldsymbol{P}_0. \tag{8}$$

3.2.2 Kalman filter formulation

For a model to capture the main tidal oscillation, it is assumed that the shallow water equations are a reasonable model for the water dynamics:

$$\begin{aligned} \frac{\partial u}{\partial t} - fv + g\frac{\partial \eta}{\partial x} &= 0 \\ \frac{\partial v}{\partial t} + fv + g\frac{\partial \eta}{\partial y} &= 0, \end{aligned} \tag{9}$$

where u and v are the eastward and northward velocity components, respectively, x and y the eastward and northward coordinates, respectively, f the Coriolis parameter, η the surface elevation and g the acceleration due to gravity. The shallow water equations (9) can be casted into

$$\begin{aligned} \frac{\partial^2 u}{\partial t^2} + f^2 u &= -g\left(f\frac{\partial \eta}{\partial y} + \frac{\partial^2 \eta}{\partial t \partial x}\right) \\ \frac{\partial^2 v}{\partial t^2} + f^2 v &= -g\left(f\frac{\partial \eta}{\partial x} + \frac{\partial^2 \eta}{\partial t \partial y}\right) \end{aligned} \tag{10}$$

The right-hand side terms in (10) can be regarded as the forcing of the system, which we try to seek. To that end, the surface level gradients are represented by harmonic functions with unknown coefficients $A_{\{x,y\}}$ and $B_{\{x,y\}}$,

$$\frac{\partial \eta}{\partial x} = A_x \cos\omega t + B_x \sin\omega t, \text{ and} \tag{11}$$

$$\frac{\partial \eta}{\partial y} = A_y \cos\omega t + B_y \sin\omega t, \tag{12}$$

where ω is the main tidal frequency (M_2, for example). The addition of more tidal frequencies is trivial, however.

Defining the dynamical system (1) the state vector is chosen as

$$\boldsymbol{x} = [A_x, B_x, A_y, B_y]^T. \tag{13}$$

Furthermore, the coefficients $A_{\{x,y\}}$ and $B_{\{x,y\}}$ are modelled as constants, so that, as an example, the process for A_x becomes

$$A_{xk} = A_{xk-1} + \text{ process noise}, \tag{14}$$

leading to the simple transition matrix

$$\boldsymbol{F} = \text{diag}(1,1,1,1). \tag{15}$$

Biogeosciences Discuss., doi:10.5194/bg-2016-118, 2016
Manuscript under review for journal Biogeosciences
Published: 11 July 2016

The measurements ($\boldsymbol{y}$) are depth averaged water velocities, averaged in time from the time of diving until the time of resurfacing. In order to determine the elements in the measurement matrix $\boldsymbol{H}$ that relates the measurements to the state vector as $\boldsymbol{y} = \boldsymbol{H}\boldsymbol{x}$, the surface elevation gradients (11) and (12) are substituted into (10), which gives the expressions for the instantaneous current components

$$u = \frac{1}{f^2 - \omega^2}\left[a_0 \cos\omega t + a_1 \sin\omega t\right] \tag{16}$$

$$v = \frac{1}{f^2 - \omega^2}\left[b_0 \cos\omega t + b_1 \sin\omega t\right] \tag{17}$$

where

$$a_0 = -gfA_y - g\omega B_x$$
$$a_1 = -gfB_y + g\omega A_x$$
$$b_0 = -gfA_x - g\omega B_y$$
$$b_1 = -gfB_x + g\omega A_y$$

The averaged currents are then found by integrating the instant current components with respect to time and dividing the result by the subsurface time T. It follows that

$$\boldsymbol{H} = \frac{g}{T(f^2 - \omega^2)}\begin{bmatrix} -C & -S & -f/\omega S & +f/\omega C \\ -f/\omega S & +f/\omega C & -C & -S \end{bmatrix}. \tag{18}$$

Herein $C = \cos(\omega t_1) - \cos(\omega t_0)$ and $S = \sin(\omega t_1) - \sin(\omega t_0)$, in which t_0 and t_1 are the dive and resurface times, respectively, and $T = t_1 - t_0$.

The measurement error is assumed to be directionally uncorrelated, so that

$$\boldsymbol{R} = r\,\mathrm{diag}(1, 1), \tag{19}$$

where r is the variance of the measurements. The numerical value can be estimated relatively easy. Factors that influence the accuracy of the measurement are the accuracy of the dive and resurface positions, and the dead-reckoning algorithm. Dive and resurface positions are derived from GPS measurements, which have a finite precision, roughly 10-20 m. However, since it takes time for a valid GPS position to be received, the resurface position and the position when the first valid GPS value is acquired do not necessarily co-locate. In addition, the dead-reckoning algorithm uses input data, such as depth rate, heading and pitch, provided by several sensors, each introducing a degree of uncertainty. A value of 1 $\mathrm{cm \cdot s^{-1}}$ is taken as a reasonable estimate for the accuracy of the depth and time averaged current measurement from the glider platform.

It is less obvious how to quantify the process noise matrix $\boldsymbol{Q}$. The process noise accounts for uncertainties in the model description of the process. Clearly, using the steady state solution of the shallow water equations, assuming the only forcing is due to the tides, the model underpinning the Kalman filter is not fully representing reality. The process noise allows for some distrust in the model description, favouring the measurements, or, put differently, it allows for flexibility of the model to adapt

Biogeosciences Discuss., doi:10.5194/bg-2016-118, 2016
Manuscript under review for journal Biogeosciences
Published: 11 July 2016

by "forgetting" old measurements. It is assumed that the process noises for each tidal component and direction is uncorrelated, so that

$$\boldsymbol{Q} = q\mathrm{diag}(1,1,1,1). \tag{20}$$

The variance parameter q is then regarded as a tuning parameter. The value is considered optimal when the variance or standard deviation of $\boldsymbol{\varepsilon}$ is minimal. The elements in $\boldsymbol{\varepsilon}$ are given by (see also (5))

$$\boldsymbol{\varepsilon}_k = \boldsymbol{y}_k - \boldsymbol{H}_k \hat{\boldsymbol{x}}_k^-, \tag{21}$$

that is, the averaged current estimate is computed from the measurement matrix $\boldsymbol{H}$ at the current level, but with the estimate for the amplitudes of the previous level/surfacing. Note that due to the virtue of (15), $\hat{\boldsymbol{x}}_k^- = \hat{\boldsymbol{x}}_{k-1}^+$.

4 Assessment of the performance of the algorithm

4.1 Instrumentation and field data

Below, data of measured currents are used to assess the performance of the current prediction algorithm. Two data sets were used for this purpose. The first data set was obtained from measured currents from a bottom mounted acoustic Doppler current profiler, from which synthetic, but realistic, depth and time averaged currents were constructed. These data time series mimick the glider data, but have predefined and controllable subsurface times. In addition, the synthetic data set removes any uncertainty introduced by the glider's dead-reckoning algorithm, rendering this a useful data set to assess the performance of the prediction algorithm *per se*. The second data set uses current estimates from glider data obtained during a field experiment. Analysing the results for both data sets allows us to quantify the effects on accuracy of the subsurface time and the glider's dead-reckoning algorithm.

The data used in this study were collected during a field experiment that took place in the German Bight, in the German sector of the North Sea in August 2014, see Figure 2a. An upwardlooking RDI Workhorse 600 kHz ADCP was bottom mounted near buoy NSB3 (54°40.7′ N, 6°47.1′ E) at about 40 m depth (Figure 2a). The deployment period ranges from 16 July 2014 until 31 August 2014. The instrument was configured with bin sizes of 40 cm yielding a current profile every 10 minutes. Each measured profile is the ensemble mean of 32 pings.

The glider *Sebastian*, a Teledyne Webb Research Slocum Electric littoral glider (Jones. et al., 2005), was deployed on 24 July 2014 and recovered on 26 August 2014. Its tracks are shown in Figure 2a. From 4 August until 10 August and from 13 August until 17 August, the glider was programmed to fly in a spiralling mode (with the steering fin set to a fixed position).

The target area for the glider operation was near the buoy NSB3 and the ADCP. Figure 2b shows that most of the time the glider was within 10 km distance from the ADCP. Therefore, the tidal currents, as well as mesoscale wind and buoyancy driven currents that are subject to the ADCP and glider measurements are expected to be the same.

Biogeosciences Discuss., doi:10.5194/bg-2016-118, 2016
Manuscript under review for journal Biogeosciences
Published: 11 July 2016

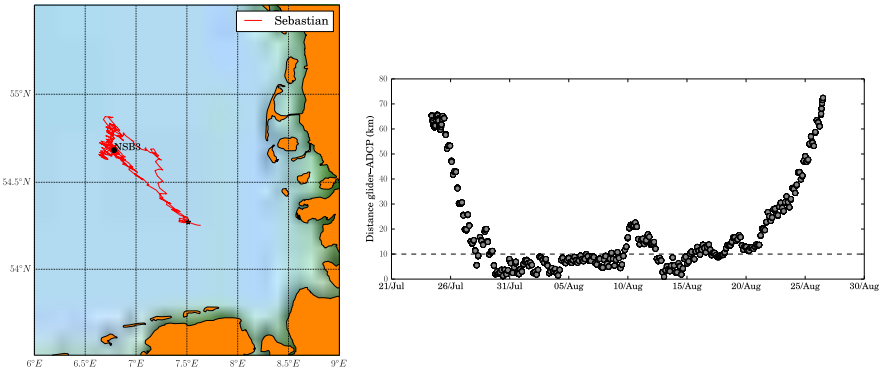

a) b)

Figure 2. Panel a) Track of glider *Sebastian* during 2014 experiment and location of the bottom mounted ADCP near buoy NSB3; panel b) distance between glider and bottom mounted ADCP.

4.2 Algorithm assessment

In order to evaluate the performance of the filter, first the ADCP measurements were used. The instantaneous currents measured with the ADCP are considered as the true currents. Synthetic glider measurement data were obtained by time and depth averaging the ADCP measurements, followed by adding white noise. The time averaging was performed over a window representing the subsurface time of the glider. This interval was set to 3 hours, which is a typical value during operations in the North Sea. Below, however, the influence of the subsurface time on the accuracy on the prediction algorithm is addressed specifically. The added noise is Gaussian with zero mean and a standard deviation of $1\ \mathrm{cm}\cdot\mathrm{s}^{-1}$.

Firstly, the synthetic measurements were low pass filtered using a second order Butterworth filter as outlined above. The purpose of this filter is to remove the main semidiurnal and faster tidal signatures. The result is shown in Figure 3 for the forward filter (red) and the phase-preserving forward-backward filter (green). The synthetic measurement data are shown in transparent blue. The figure shows that the residual current does not vary too much, except for a few short periods, notably in the northward current. One of these periods with significant variation in the residual current is the time window of some 3 days starting at 10 August, which can be linked to the passage of a low pressure system (remnants of the hurricane "Bertha"). The graphs clearly show that, compared to the forward-backward filter, the forward filter introduces a phase lag of about 10 hours, which has immediate consequences for the accuracy with which the currents can be estimated during these conditions.

Secondly, the synthetic current measurements, corrected for the residual current using the low pass filtered currents, were subjected to the Kalman filter. The initial conditions were set by the state vector $\boldsymbol{x}_0 = [0,0,0,0]^T$ (zero tidal amplitude components) and a high covariance matrix $\boldsymbol{P}_0 = \mathrm{diag}(1000,1000,1000,1000)\ \mathrm{m}^2\cdot\mathrm{s}^{-2}$, which signifies that the current state of the system is unknown. Furthermore, the measurement noise variance parameter was set to $r = 1\times10^{-4}\ \mathrm{m}^2\cdot\mathrm{s}^{-2}$, in correspondence to the added noise, $r = \sigma^2$.

Biogeosciences Discuss., doi:10.5194/bg-2016-118, 2016
Manuscript under review for journal Biogeosciences
Published: 11 July 2016

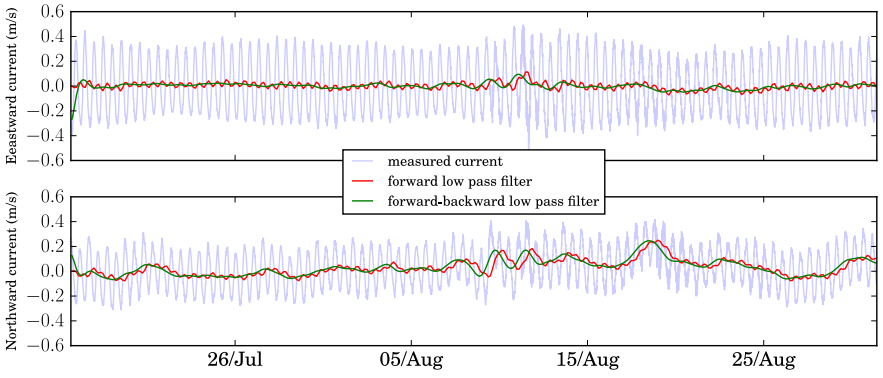

Figure 3. Eastward and northward currents are shown in the top and bottom panel, respectively. The synthetic 3-hour averaged currents are shown in transparent blue, and the forward and forward-backward filtered residual currents are shown in red and green, respectively.

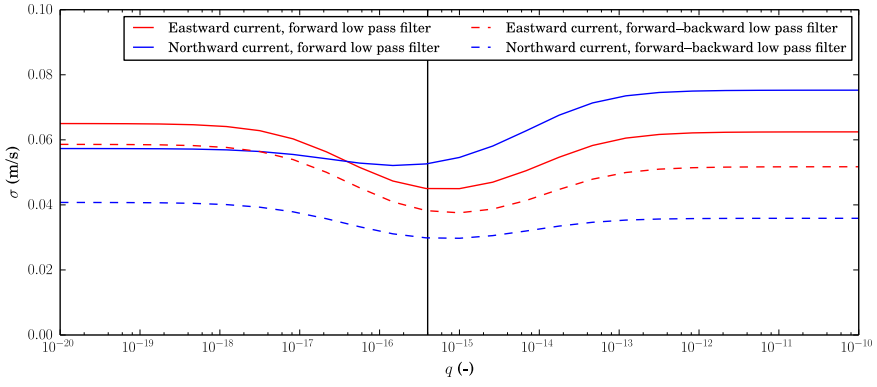

Figure 4. Standard deviations of the errors of the eastward (blue) and northward (red) current components, as a function of the variance parameter q (process noise). The solid lines were obtained using a forward low pass filter to remove the residual current (near-real time mode), whereas the dashed lines were obtained using a forward–backward low pass filter (delayed mode). The black line indicates $q = 4 \times 10^{-16}$, which is the optimal value taking into account eastward and northward currents as well as near-real time and delayed mode scenarios.

In order to find the optimal value for the variance parameter q, the Kalman filter was run for a number of different values of q. The Kalman filter yielded the lowest standard deviation of the error in the estimated currents in both near-real time mode and delayed mode (see Section 5) for $q \approx 4 \times 10^{-16}$, see Figure 4. The value of $q = 4 \times 10^{-16}$ is used throughout this work.

The Kalman filter (2) – (6) was updated when a new current measurement becomes available, *i.e.* at 3 hour intervals. The error of the estimate of the depth and time averaged current components for each time step is given by (21). The results are summarised in histograms in Figure 5. The top and bottom left panels show the histograms of the eastward and northward

Biogeosciences Discuss., doi:10.5194/bg-2016-118, 2016
Manuscript under review for journal Biogeosciences
Published: 11 July 2016

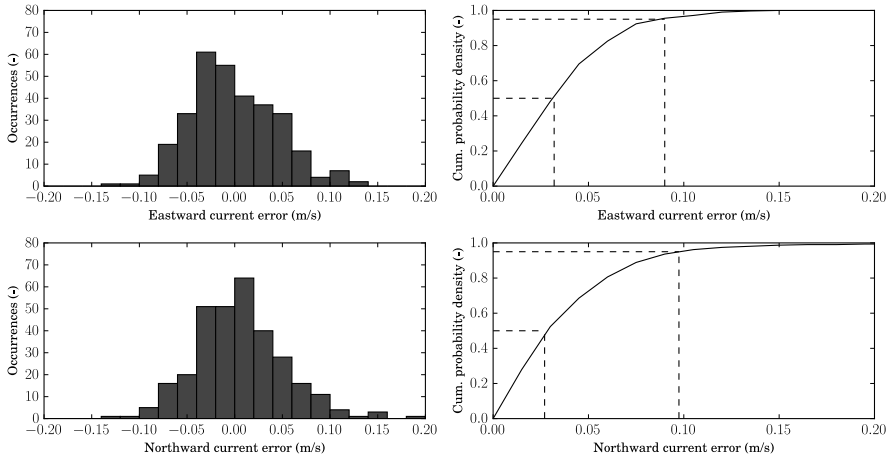

Figure 5. Errors in the estimated currents. Upper left panel: histogram for eastward direction, bottom left panel: histogram for northward direction, upper right panel: estimated probability density function for eastward current, and bottom right panel: estimated probability density function for northward current. The dashed lines indicate the 50% and 95% levels.

currents, respectively. The distributions of the errors seem Gaussian and have standard deviations of 4.5 and 4.9 $\mathrm{cm \cdot s^{-1}}$ for the eastward and northward currents, respectively. The means are ≈ 0 for both the eastward and northward components. The panels on the right-hand side show the cumulative probability density. The mean error is approximately 2.9 $\mathrm{cm \cdot s^{-1}}$. Furthermore, 95% of the estimates have an error margin smaller than 9.0 and 9.7 $\mathrm{cm \cdot s^{-1}}$ for the eastward and northward components, respectively.

The instantaneous current components are readily computed once the amplitude estimates of the tidal components are computed. Figure 6 shows an example of a 17-day period of instantaneous currents. In particular for the north component, two instances where the residual current changes in time are discernible, namely around 8 and 18 August. Due to the lagging response of the Butterworth filter, the estimated currents deviate most from the measured currents when sudden changes occur in the residual currents.

Having applied the current prediction algorithm to the synthetic current measurements, mimicking glider subsurface times of 3 hours, it can be concluded that the algorithm predicts the depth and time integrated current within 9 $\mathrm{cm \cdot s^{-1}}$, and with an average error of about 4-5 $\mathrm{cm \cdot s^{-1}}$. The sources of these errors are the decomposition of the currents into residual and tidal currents by low pass filtering on the one hand, and the oversimplified tidal currents model on the other.

In practice, the errors due to the dead-reckoning algorithm that get absorbed into the current measurements by the glider, will degrade the performance of the current prediction algorithm. To quantify this degradation, the algorithm is applied to the observed current measurements from the glider, and compared with the currents as measured by the ADCP, which are considered

Biogeosciences Discuss., doi:10.5194/bg-2016-118, 2016
Manuscript under review for journal Biogeosciences
Published: 11 July 2016

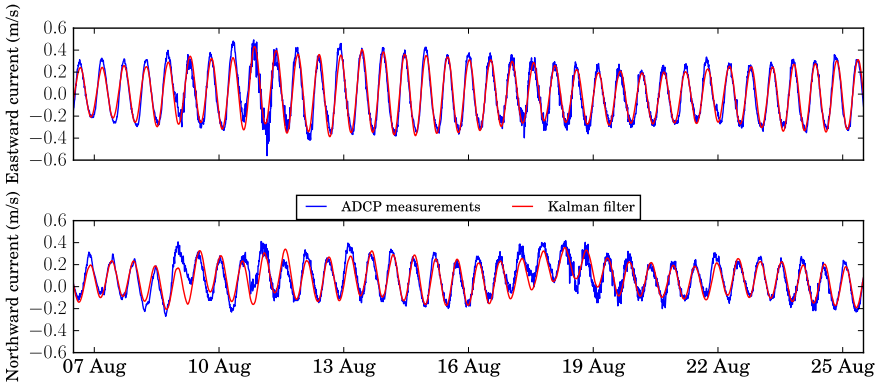

Figure 6. 17-Day time series of measured currents and Kalman filter estimated currents for the eastward component (top panel) and the northward panel (bottom panel).

the ground truth. Since the glider operated within 10 km of the ADCP during most of the mission time, see Figure 2b, this seems a reasonable assumption.

In contrast to the synthetic data, the glider data do not have a fixed interval. For the present glider dataset, most of the subsurface times were between 2.6 and 3.0 hours, as during most of the mission the glider was programmed to resurface at three hour intervals, interpreted as resurface time-to-resurface time. The reason for the mean subsurface time to be less than 3 hours is due to the fact that at resurfacing the glider spent about 10-15 minutes afloat to transmit data. Leaving all parameter settings of the low pass filter and the Kalman filter unchanged, the depth and time averaged current estimates are compared with those computed from the ADCP current measurements, where time intervals for averaging the ADCP data were matched to the factual subsurface times of the glider. The results are summarised in Figure 7. In this figure the left panel represents the eastward current error and the right panel the northward current error. Comparing the near-real time glider data results (black curves), that is forward-filtered only, with the results of the synthetic dataset from ADCP data (red curves), it is seen that the performance dropped, as expected. On average the errors (50% and 95% levels) increase by a factor of 1.3.

The near-real time current estimates are potentially useful for assimilation into circulation models, see for example Stanev et al. (2015). Every time the glider surfaces, the Kalman filter can be run, using the latest available measurement estimate of the depth and time averaged current. Since the state vector $\boldsymbol{x}$ contains the amplitudes of the surface slopes of the main tidal components, the instantaneous currents can easily be computed from (16) and (17), which yield a more applicable measure for the current than a time averaged value. Comparing the estimates of the instantaneous current components with the instantaneous currents measured with the ADCP, the standard deviations of the (depth averaged) currents amount to 6.6 and 6.8 $\mathrm{cm \cdot s^{-1}}$ for the eastward and northward components, respectively, see also Table 1.

Biogeosciences Discuss., doi:10.5194/bg-2016-118, 2016
Manuscript under review for journal Biogeosciences
Published: 11 July 2016

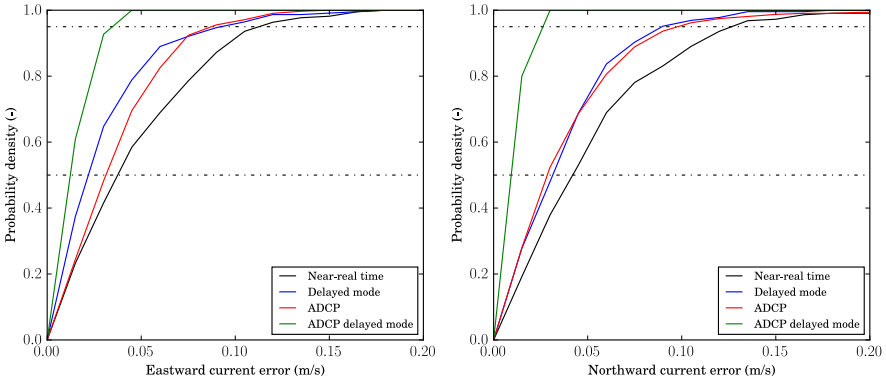

Figure 7. Probability density function estimates of the errors for the eastward current component (left panel) and the northward component (right panel). The black and red curves are derived from the results of the Kalman filter run in near-real time mode for the glider data and ADCP data, respectively. The blue and green curves are derived from the Kalman filter modified for delayed mode (post-processing), see Section 5.

5 Glider derived currents in delayed mode (post-processing)

The approach proposed herein can also be used to reprocess the glider data to obtain estimates of the instantaneous barotropic currents once the glider mission has been completed. In delayed mode, a number of improvements can be applied. First, the depth and time averaged current estimates can be improved by recalculating the dead-reckoned position. The glider's dead-reckoning algorithm computes the horizontal velocity component from the pitch and the pressure rate, ignoring the angle of attack. Although the angle of attack is generally small, the glider algorithm may overestimate its horizontal speed by a few $\mathrm{cm}\cdot\mathrm{s}^{-1}$. An improved dead-reckoning calculation can be done post-mission by implementing the dynamical glider model of Merckelbach et al. (2010).

Second, a significant source of error in the estimated currents is the phase lag introduced by the Butterworth filter, see Section 3.1. This effect can be mitigated by running the filter forwards and backwards in time, as demonstrated in Figure 3.

Third, a Kalman filter can be formulated that uses both "historic" and "future" observations. To that end the Kalman filter described above is run forward and backward, whereas the final estimate of the vector $\hat{\boldsymbol{x}}_k$ for time index k is combined from the forward and backward quantities (Simon, 2006):

$$\boldsymbol{K} = \boldsymbol{P}^{-}_{\mathrm{b},k}(\boldsymbol{P}^{+}_{\mathrm{f},k} + \boldsymbol{P}^{-}_{\mathrm{b},k})^{-1}, \tag{22}$$

$$\hat{\boldsymbol{x}}_k = \boldsymbol{K}\boldsymbol{x}^{+}_{\mathrm{f},k} + (\boldsymbol{I} - \boldsymbol{K})\boldsymbol{x}^{-}_{\mathrm{b},k}, \tag{23}$$

where the subscripts "f" and "b" denote forward and backward filter results, respectively.

Figure 7 shows the improvement achieved due to additional backward filtering step. For both the synthetic and the glider data sets, the errors in the depth and time averaged currents are reduced. The averaged factor of improvement for the glider

Biogeosciences Discuss., doi:10.5194/bg-2016-118, 2016
Manuscript under review for journal Biogeosciences
Published: 11 July 2016

	Eastward current		Northward current	
	μ ($\mathrm{cm \cdot s^{-1}}$)	σ ($\mathrm{cm \cdot s^{-1}}$)	μ ($\mathrm{cm \cdot s^{-1}}$)	σ ($\mathrm{cm \cdot s^{-1}}$)
near-real time	-1.0	6.6	-0.9	6.8
delayed mode	-0.1	4.9	-0.9	4.8

Table 1. Means and standard deviations of instantaneous current estimates in near-real time and delayed mode.

data (synthetic data) is approximately 1.7 (2.6). The improvement for the instantaneous current estimates is similar and yields a standard deviation of less than 5 $\mathrm{cm \cdot s^{-1}}$, see Table 1.

6 Virtual AIS

Developed in the 1990's, the automatic identification system (AIS), which is based on VHF radio communications, allows ships to both see and be seen by other marine traffic in their area. The system augments radar and has increased the safety at sea. Since AIS instrumentation is generally bulky and would take a substantial cut from the glider's energy resources, and the fact that AIS signals do not penetrate water, it is for technical reasons not feasible to equip a glider with an AIS transmitter. Being able to broadcast its position to surrounding ships would, however, reduce the probability of a collision between a glider and a ship drastically. An alternative to AIS is virtual AIS, whereby the position of an object (glider) is broadcasted from an AIS transmitter elsewhere (a land station). In Germany the authority Wasser-und-Schifffahrtsverbund (WSV) regulates the use of virtual AIS, and has shown interest in this approach.

The principle of operation of a virtual AIS system is as follows. Two situations are discerned, namely the period when the glider is at the surface, and when it is underwater. When the glider is at the surface, and has established a (satellite) communication link with a server on shore, its actual GPS position is known. This information is instantly and automatically relayed to an operator room of WSV, from which the positional information of the glider is broadcasted as an AIS message. When the glider is underwater, and no actual GPS position is available, an estimated position can be broadcasted. To estimate a position, information is required on the local current field, and the behaviour of the glider in terms of hardware behaviour (how it is programmed and responses), and the dynamic behaviour (how and how fast it flies through the water). The modelling of the glider behaviour is considered beyond the scope of this study and therefore not discussed.

Assuming an adequate model of the glider behaviour is available, it is expected that the uncertainty in the underwater glider position grows the longer it is underwater. The synthetic data set can be used to quantify the effect of subsurface time on the uncertainty in position, as this dataset can easily be divided in predefined subsurface times. Running the (forward) filter repeatedly for subsurface times, spanning 12 hours with 10 minute intervals, ensembles of six consecutive runs are formed.

Figure 8 shows the ensemble averaged errors in estimated position for the mean, the 75 and 95 percentile errors, drawn by blue, green and red solid curves, respectively. The identically shaded areas indicate the variation present in each ensemble. As anticipated the errors increase with increasing subsurface time. Because of the longer integration times, the errors in the

Biogeosciences Discuss., doi:10.5194/bg-2016-118, 2016
Manuscript under review for journal Biogeosciences
Published: 11 July 2016

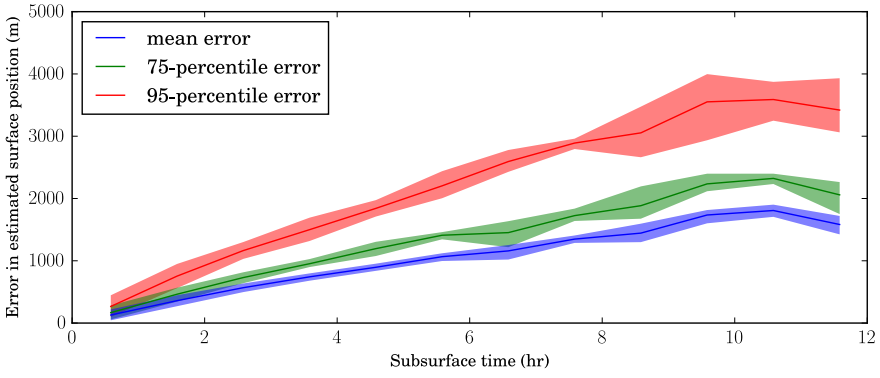

Figure 8. Error in estimated resurfacing position as a function of subsurface time.

estimated velocities in fact reduce slightly with increasing subsurface time, expressed by the flattening of the curves for longer subsurface times.

As the position error increases from zero at the time of diving, the errors shown in Figure 8 are the maximum errors, *i.e.* the expected errors just prior to resurfacing. Depending on the required limit of this error, the maximum allowable subsurface time can be defined. Here the data suggest that for a subsurface time of 3 hours, the average error is less than 650 m and that virtually all estimates are within double that distance.

Presently, this system is not implemented yet. The authority WSV has expressed its interest, and also indicated that the errors in the prediction for 3 hourly dives are acceptable. Technical limitations of the AIS system in use by WSV prevents a (semi-)automatic implementation. Furthermore, the range of the landstations to broadcast the AIS messages is limited to about 70 km offshore, and would not reach far enough to cover the outerparts of the German sector of the German Bight.

7 Discussion

The approach presented herein comes with a number of advantages. First, with a focus on glider path prediction, previous experience has shown that an unjustifiable amount of effort is required to guarantee current model output to be available at all times. Using glider estimated currents removes this vulnerability, as this information is always available, assuming a glider operates normally. Second, the proposed algorithm provides independent estimates of the instantaneous currents. In near-real time these estimated currents can be assimilated into the COSYNA-run ocean current models of the German Bight, in a similar fashion as radar observations of surface currents are assimilated (Stanev et al., 2015).

In delayed mode, when all data are available, the accuracy of the current estimates can be further improved. Still, the accuracy would remain inferior to the accuracy that can be achieved with direct measurements from devices such as ADCPs. However, as often, for practical and logistical reasons, few, if any at all, independent current data are available that co-locate with glider data, so that a third advantage is that for many applications the improved glider based current estimates may be the

Biogeosciences Discuss., doi:10.5194/bg-2016-118, 2016
Manuscript under review for journal Biogeosciences
Published: 11 July 2016

only information on instantaneous currents available. Thus, this method may allow the aspect of mixing being incorporated in the data analysis, which is crucial for the interpretation of observations of phytoplankton blooms (e.g., Xu et al., 2013), sediment resuspension events (e.g., Glenn et al., 2008), or oxygen depletion events (e.g., Queste et al., 2106).

We chose to decompose the currents into a tidally driven part and a residual current. Lacking a realistic model for the residual currents, this component was quantified by a simple low pass filter, whereas the tidally driven currents were estimated using a Kalman filter based on the shallow water equations. Instead of this approach, a variety of other formulations could have been considered.

Instead of using a low pass filter, a Kalman filter for the residual current could be formulated based on the model

$$\dot{\boldsymbol{u}}_{\mathrm{r}} = 0 \tag{24}$$

where the subscript "r" refers to residual. This model states that the current is constant. The Kalman filter will update the prediction of the current with every new measurement. How much the measurements are trusted over residual current modelled as a constant, depends on the predefined model noise. Similar to the forward low pass filter, this Kalman filter introduces a lag, the magnitude of which depends on the model uncertainty. As the purpose of this Kalman filter is to filter out the residual component of the current, it is not straight forward to set the process noise such that right model stiffness is achieved. This is in contrast with the low pass filter, the behaviour of which is well-defined given the order and the cut-off frequency. If the model would be based on the assumption that $\dot{\boldsymbol{a}}_{\mathrm{r}} = 0$, the same arguments still would apply, although this variant has the advantage that between measurements the estimated residual current is assumed to vary linearly, rather than being constant.

A different approach could be to incorporate the residual current Kalman filter based on (24) directly in the Kalman filter developed in Section 3.2, by modifying (15)–(18). The major drawback of this formulation is that the filter has no means to discriminate between the residual and tidal components of the measured currents, other than specifying different model noises for the tidal and residual current models and may therefore not converge. In conclusion, applying a low pass filter to the measured currents to separate the residual and tidal current components is the simplest and most robust approach, and therefore preferred.

The current estimation algorithm described herein could also be implemented on board a Slocum glider to benefit its underwater navigation capabilities in tidal waters. However, as the navigation software of the Teledyne Slocum glider is closed-source, this has not been pursued. If the algorithm were to be implemented, the key advantage would be that the glider would be able to keep a straighter course during its mission, which would facilitate the data analysis. As the algorithm would not fare well in regions that are not dominated by the tides, the usefulness of such an implementation is limited to the relatively small coastal glider community, and unlikely to materialise.

8 Conclusions

Although the navigational algorithm implemented on board the (Slocum) glider yields depth and time averaged currents, the time resolution, set by the subsurface time, is often too coarse for the purpose of data analysis. This is particularly the case

Biogeosciences Discuss., doi:10.5194/bg-2016-118, 2016
Manuscript under review for journal Biogeosciences
Published: 11 July 2016

in regions where the currents are dominated by the tides. In this work an algorithm, tailored to coastal seas with strong tidal currents, was presented that can be used to estimate the instantaneous currents from the time averaged current measurements obtained by the glider. The algorithm considers a current component driven by the tides, and a residual current, varying on longer timescales than the main (semidiurnal) tides.

During the mission, the algorithm can be used to predict the currents, which is essential to make a projection of the glider trajectory up to 12 hours or so ahead. Run as a predictive tool, both the low pass filter and the Kalman filter are run forward in time only, which inevitably leads to lagging effects. This is particularly apparent in the residual currents resulting from the low pass filter. For a typical application of a glider run in the North Sea, a second order Butterworth filter was chosen as a trade-off between the width of the transition band and the group delay. To achieve the required amount of damping of the semidiurnal tidal signals and their higher harmonics, a group delay of about 10 hours needs to be accepted.

To assess its performance, the algorithm was first applied to depth and time averaged currents, constructed from instantaneous currents measured with an ADCP, with known noise levels added (synthetic data). By averaging over time, information is lost, so that the measurements presented to the Kalman filter contain less information than the original ADCP measurements. The loss of this information is mostly compensated by information provided by the shallow water model. For an anticipated subsurface time of 3 hours, the correlation coefficients calculated for the estimated and ADCP measured instantaneous currents were found to be 0.97 and 0.94 for the eastward and northward components, respectively. This result indicates that the algorithm as such lives up to the expectations and is capable of reconstructing the instantaneous currents to a large extent.

When applied to the glider derived current measurement, and compared with ADCP data measured within a radius of about 10 km, the algorithm performs slightly worse, with correlation coefficients of 0.96 and 0.90 for the eastward and northward current components, respectively. This regression is attributed to the additional uncertainty caused by the navigation algorithm. Still, for subsurface times of three hours, which is a typical operational setting, the estimate of the instantaneous current has standard deviation of 6-7 $\mathrm{cm \cdot s^{-1}}$, which is considered low enough to be used for data assimilation procedures.

A further application could be to incorporate the present algorithm in a virtual AIS system to enhance the safety at sea. Herein the glider's position between surfacings can be estimated. The uncertainty in the estimated position grows with the time that the glider is underwater. Quantifying the effect of the uncertainty in the currents on the positional accuracy, it was found that subsurface times up to 3 hours would yield a positional accuracy that was still acceptable for the German authority Wasser-und Schifffahrtsverbund.

In delayed mode, the performance of the algorithm can be increased by running the low pass filter and the Kalman filter in forward-backward mode. The backward run in effect counters the lag introduced in the forward sweep. The standard deviation of the instantaneous current estimate was found to drop below 5 $\mathrm{cm \cdot s^{-1}}$. This means that for the purpose of data analysis, where the (depth-averaged) current is often regarded as an important driving force, the proposed algorithm provides a way to reconstruct the instantaneous currents with a sufficiently degree of accuracy.

Acknowledgements. This work was jointly financially supported by GROOM of the 7th Framework Programme of the European Union under Grant Agreement No 284321, and through the Coastal Observing System for Northern and Arctic Seas (COSYNA).

Biogeosciences Discuss., doi:10.5194/bg-2016-118, 2016
Manuscript under review for journal Biogeosciences
Published: 11 July 2016

References

Baschek, B., Brix, H., Badewien, T., Breitbach, G., Colijn, F., Doerffer, R., Emeis, K.-C., Eschenbach, C., Friedrich, J., Fischer, P., , Garthe, S., Horstmann, J., Ohle, N., Petersen, W., Riethmüller, R., Röttgers, R., Schlüter, M., Schroeder, F., Schulz-Stellenfleth, J., Seemann, J., Stanev, E., Winter, C., Wirtz, K., Zielinski, O., and Ziemer, F.: COSYNA – Coastal Observing System for Northern and Arctic Seas, Ocean Sciences, 2016.

Drücker, S., Steglich, D., Merckelbach, L., Werner, A., and Bargmann, S.: Finite element damage analysis of an underwater glider–ship collision, Journal of Marine Science and Technology, pp. 1–10, doi:10.1007/s00773-015-0349-7, 2015.

Garau, B., Bonet, M., Alvarez, A., Ruiz, S., and Pascual, A.: Path Planning for Autonomous Underwater Vehicles in Realistic Oceanic Current Fields: Application to Gliders in the Western Mediterranean Sea, Journal of Maritime Research, 6, 5–22, 2009.

Glenn, S., Jones, C., Twardowski, M., Bowers, L., Kerfoot, J., Kohut, J., Webb, D., and Schofield, O.: Glider observations of sediment resuspension in a Middle Atlantic Bight fall transition storm, Limnology and Oceanography, 53, 2180–2196, 2008.

Johnston, T., Rudnick, D., Alford, M., Pickering, A., and Simmons, H.: Internal tidal energy fluxes in the South Chinae Sea from density and velocity measurements by gliders, J. Geophys. Res., 118, 3939–3949, 2013.

Jones., C., Creed, E., Glenn, S., Kerfoot, J., Kohut, J., Mudgal, C., and Schofield, O.: Slocum gliders - a component of operational oceanography, Proc. UUST, Autonomous Undersea Systems Institute, 2005.

Merckelbach, L.: On the probability of underwater glider loss due to collision with a ship, J Mar Sci Techonol, 18, 75–86, doi:10.1007/s00773-012-0189-7, 2013.

Merckelbach, L., Briggs, R., Smeed, D., and Griffiths, G.: Current measurements from autonomous underwater gliders, in: Proceedings of the IEEE/OES/CMTC Ninth Working Conference on Current Measurement Technofogy, pp. 61–67, IEEE, 2008.

Merckelbach, L., Smeed, D., and Griffiths, G.: Vertical velocities from underwater gliders, Journal of Oceanic and Atmospheric Technology, 27, 547–563, 2010.

Oppenheim, A. V., Willsky, A. S., and Nawab, S. H.: Signals and Systems, Prentice Hall, second edition edn., 1997.

Queste, B., Fernand, L., Jickells, T., Heywood, K., and Hind, A.: Drivers of summer oxygen depletion in the central North Sea, Biogeosciences, 13, 1209–1222, doi:10.5194/bg-13-1209-2016, 2106.

Rippeth, T. P., Palmer, M. R., Simpson, J. H., Fisher, N. R., and Sharples, J.: Thermocline mixing in summer stratified continental shelf seas, Geophysical Research Letters, 32, doi:10.1029/2004GL022104, 2005.

Rudnick, D. L.: Ocean Research Enabled by Underwater Gliders, Annu. Rev. Mar. Sci., 8, 519–541, doi:10.1146/annurev-marine-122414-033913, 2016.

Simon, D.: Optimal State Estimation, Wiley and Sons, 2006.

Simpson, J. and Hunter, J.: Fronts in the Irish Sea, Nature, 250, 404–406, doi:10.1038/250404a0, 1974.

Smith, R., Chao, Y., Li, P., Caron, D., Jones, B., and Sukhatme, G.: Planning and implementing trajectories for autonomous underwater vehicles to track evolving ocean processes based on predictions from a regional ocean model, International Journal of Robotics Research, 29, 1475–1497, 2010.

Smith, R. N., Kelly, J., and Sukhatme, G. S.: Towards improving mission execution for autonomous gliders with an ocean model and Kalman filter, IEEE International Conference on Robotics and Automation (ICRA), pp. 4870–4877, doi: 10.1109/ICRA.2012.6224609, 2012.

Biogeosciences Discuss., doi:10.5194/bg-2016-118, 2016
Manuscript under review for journal Biogeosciences
Published: 11 July 2016

Stanev, E. V., Ziemer, F., Schulz-Stellenfleth, J., Seemann, J., Staneva, J., and Gurgel, K.-W.: Blending Surface Currents from HF Radar Observations and Numerical Modeling: Tidal Hindcasts and Forecasts, J. Atmos. Oceanic Technol., 32, 256–281, doi:10.1175/JTECH-D-13-00164.1, 2015.

Tropp, M.: Analysis of resuspension of sediment from underwater glider observations, Master's thesis, Institute of Oceanography, University of Hamburg, 2013.

Xu, Y., Cahill, B., Wilkin, J., and Schofield, O.: Role of wind in regulating phytoplankton blooms on the Mid-Atlantic Bight, Continental Shelf Research, 63(Suppl.), S26–35, doi:10.1016/j.csr.2012.09.011, 2013.